Advanced Energy and Sustainability Research

ADVANCED ENERGY & SUSTAINABILITY RESEARCH Open Access

www.advenergysustres.com

RESEARCH ARTICLE OPEN ACCESS

Voltage and Cation Dependent Electron Storage in Carbon Nitride as Blue K-PHI by Electrochemical Loading

Shilin Yang[1] | Leonardo Cancellara[1] | Abraham Kasa[1,2,3] | Markus Antonietti[1] | Mateusz Odziomek[1] | Horațiu Szalad[1]

[1]Department of Colloid Chemistry, Max Planck Institute of Colloids and Interfaces, Research Campus Golm, Potsdam, Germany | [2]Hasselt University, Imo-imomec, Hasselt, Belgium | [3]Imec, Energyville, Genk, Belgium

Correspondence: Horațiu Szalad (horatiu.szalad@mpikg.mpg.de)

Received: 7 May 2026 | **Revised:** 15 June 2026 | **Accepted:** 29 June 2026

Keywords: cation-effect | electrocharging | poly(heptazine imide) | semiconductors

ABSTRACT

The ability of diverse carbon nitride materials to store electrons and develop a blue color through unbalanced consumption of half-charges is well described to occur during photocatalytic reactions. Herein, a similar effect was observed and quantified via electrochemical biasing of a poly(heptazine imide) (PHI)-based electrode in organic media containing various electrolyte species. Thus, by instrumentalizing Faradaic processes in the conduction band of PHI, electron storage is observed, the amount and voltage of which depend on the density of states of the material. Thus, a maximum charge density of 82 $C\,g^{-1}$ was achieved after charging the PHI-based electrode for 30 s at an applied potential of −1.9 V versus Ag/Ag^+. Notable performance differences arose from screening different organic electrochemical media, mainly influenced by the physicochemical characteristics of chosen cationic species and organic solvent. Our herein contribution describes a novel approach to achieving a bias-dependent chromatic effect of PHI-based materials, with implications in e^- accommodation rates and outputs, and potential prospects for electrocatalytic chemical transformations.

1 | Introduction

Carbon nitrides and related heptazine-based polymers have emerged as versatile semiconductors for photocatalytic [1–3] and photoelectrochemical [4–6] energy conversion. A peculiarity that stands apart in comparison with other conventional semiconductor catalysts is described as the ability of melem-based polymeric networks, particularly poly(heptazine imide) (PHI), to run either reductive or oxidative processes in an alternating sequence, as such materials can buffer to a large extent photogenerated electrons [7, 8]. In the ideal case of fast oxidation kinetics, electrons accumulate in the semiconductor nanostructure, resulting in a distinctive photochromic phenomenon in which the catalyst changes optically from mainly yellow to distinctively blue. Under photocatalytic conditions, this electron-loaded state can be achieved when photogenerated holes are consumed rapidly, allowing electrons to persist in the material, even in the absence of incident irradiation, and to be used subsequently in delayed reduction processes, conditioned by thermodynamic requirements for the chemical conversion of said substrate. This nonconventional approach was later denoted "dark photocatalysis" [9] and was employed for time-delayed reactions such as H_2 evolution [10, 11], O_2 reduction to H_2O_2 [12, 13], and the reduction of organic substrates [14, 15]. The number of stored charges at the beginning of such studies was reported to be relatively low, corresponding to only one uncoupled e^- per nine to ten heptazine units [11] in melem-based polymeric networks, although later studies increased this value for other carbon nitride polymorphs by more than a factor of two, reaching approximately one stored electron per four heptazine units [8]. Altogether, these findings established PHI as an unusual class of light absorbers combining photoactivity with intrinsic charge-storage capability.

Beyond photochemical charging, previous work also showed that PHI can be charged electrochemically in aqueous media by application of a negative bias, under assistance of incident light irradiation [16]. In that case, the amount of stored charge depends on the attained potential and on the nature of the compensating cation. Importantly, that study was developed in the context of a solar-battery concept, employed a 2D cyanamide-functionalized PHI (NCN-PHI), and remained confined to aqueous electrolytes, where the accessible cathodic window and charge-storage behavior are inherently shaped by water-based interfacial chemistry. By contrast, the behavior of more conventional K-PHI materials under purely electrochemical charging in non-aqueous media remains insufficiently understood. This question is important because moving from water to organic electrolyte does not merely expand the reductive window; it also changes ion pairing [17], solvation [18], and interfacial charge-compensation processes [19] that are expected to influence both the amount and rate of stored charge.

Here, we focus exclusively on the electrochemical generation of the blue charged state in non-aqueous media, where broader reductive stability and different ion-solvation environments offer a distinct regime for PHI charging. In this context, we ask how the applied bias, cation identity, solvent, and electrolyte concentration govern the extent and kinetics of electron storage in freeze-dried, mechanically exfoliated K-PHI (FK-PHI) films. Our aim is not to re-establish the existence of electrochemical charge storage in PHI, but rather to determine how the extent and rate of electron accumulation depend on the applied bias and on the properties of the electrolyte environment. Specifically, we examine the influence of cation identity, solvent, and electrolyte concentration on the charging behavior of FK-PHI in organic media.

Using this approach, we show that FK-PHI can be driven rapidly into the blue electron-loaded state in organic electrolyte, reaching charge densities of up to $82\,C\,g^{-1}$ after 30 s of potentiostatic charging at −1.9 V versus Ag/Ag^{+}. We find that the charging response depends strongly on the electrochemical environment, with marked differences between Li^{+}, Na^{+}, and tetrabutylammonium-based electrolytes, as well as clear solvent effects. To probe the charged state, we combine electrochemical analysis with optical spectroscopy and in-situ electron energy-loss spectroscopy (EELS). Taken together, the data support a picture in which electrochemical bias injects electrons into the PHI framework, while the achievable charge density and discharge behavior are governed by coupled ion-electron compensation processes that are highly sensitive to the surrounding electrolyte. Thus, this work extends electrochemical PHI charging into the non-aqueous regime and clarifies how external electrochemical conditions control the formation and stability of the blue stored-electron state.

2 | Results and Discussion

2.1 | Material Preparation and Structural Validation of FK-PHI

A standard K-PHI sample was synthesized via a previously reported procedure, essentially involving the polycondensation of heptazine-based framework in a eutectic salt flux [20] (Figure 1a). Specifically, a 5-aminotetrazole precursor was thoroughly combined with LiCl and KCl, the mixture, which was thereafter thermally treated at 600°C under N_2 gaseous atmosphere to yield the desired crystalline carbon nitride analogue. After washing, the sample was mechanically exfoliated via intense ultrasound-sonication in an aqueous dispersion and freeze-dried under vacuum. The final product is denoted as FK-PHI. A schematic diagram illustrating this synthetic protocol is displayed in Scheme 1.

The final FK-PHI product was chemically, structurally, and morphologically characterized in comparison with the non-exfoliated

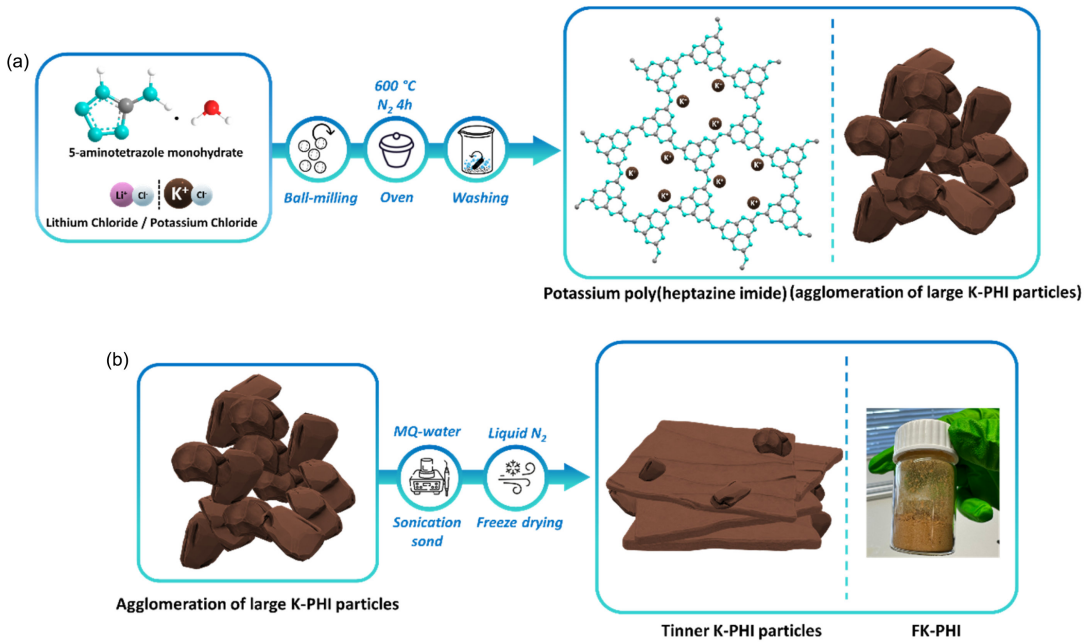

SCHEME 1 | (a) Illustration of the synthetic protocol followed for the synthesis of K-PHI, followed by (b) mechanical exfoliation and freeze-drying, which yields FK-PHI.

sample (K-PHI). HR-TEM surveys of samples under investigation highlight a successful textural alteration achieved for the FK-PHI analogue, as compared to the parent K-PHI (Figure 1a–c). Comparing micrographs of these two specimens reveals slightly altered morphologies, as large rod-like crystalline domains with strong agglomeration are observed in the case of K-PHI, whereas thinner units that retain a large degree of crystallinity are evident for the FK-PHI sample. It must be noted that, due to this strong agglomeration between particles in both cases, differentiation of domain edges is difficult to assess. The efficacy of the freeze-drying pretreatment is further supported by N_2 physisorption measurements of these samples. As shown in Figure 1d, FK-PHI exhibits higher N_2 uptake than K-PHI, corresponding to calculated specific surface areas of 93 and 54 $m^2 g^{-1}$, respectively. It must be noted that, despite this difference not being substantial, FK-PHI may exhibit larger effective surface areas upon redispersion and subsequent casting onto electrode substrates, as this processing would perturb the particle agglomeration observed under TEM screening.

PXRD diffraction patterns of investigated samples reveal characteristic crystalline reflexes associated with poly(heptazine imide) networks (Figure 1e). The in-plane order of repeating heptazine units appears unperturbed after the mechanical exfoliation protocol, as both K-PHI and FK-PHI exhibit a well-developed diffraction line at 8.15°(2θ) associated with the (100) in-plane repeat, and an additional crystalline mode at 14°(2θ) corresponding to the (110) reflection [21]. Notably, substantial diminishing of the (002) stacking reflection at 28.2°(2θ) is apparent for FK-PHI, further confirming the successful K-PHI delamination to thinner particles without structural disintegration of the polyheptazine framework. Additionally, FT-IR spectra of all investigated samples (Figure 1f) exhibit vibrational contributions at 801 cm^{-1}, characteristic of out-of-plane bending modes of heptazine units, and a broad absorption feature between 1200 and 1650 cm^{-1} arising from C—N and C═N stretching vibrations in the heterocyclic frameworks [22]. For K-PHI and FK-PHI, the band present at 987 cm^{-1} denotes the presence of K^+ cations in the nitrogen-rich structural cavities of poly(heptazine imide) [23]. Notable chemical significance must be attributed to signals appearing at 2190 cm^{-1} that correlate with edge-terminating —C≡N functionalities [24], which exhibit similar contribution for both analogs, and furthermore indicate that exfoliation occurs without major in-plane covalent alterations.

Taken together, these results show that the freeze-drying/exfoliation treatment modifies the texture and morphology of K-PHI without altering the essential PHI framework, thus providing a suitable model material for probing electrochemical charge storage in non-aqueous media.

2.2 | Electrochemical Generation of the Blue Charged State in Non-Aqueous Electrolyte

Having established the structural integrity of FK-PHI, we next examined whether the material can be driven electrochemically into the characteristic blue charged state in a non-aqueous environment. FK-PHI was deposited on conductive FTO substrates, with carboxymethyl cellulose (CMC) as a binder, and tested in acetonitrile-based electrolyte, chosen to provide a broader cathodic stability window than water and thereby allow access to more negative charging potentials. In addition, it is a common solvent used for photocatalysis of organic substrates.

Cyclic voltammetry revealed that the FK-PHI film remains visually unchanged at modest cathodic bias, but undergoes a gradual

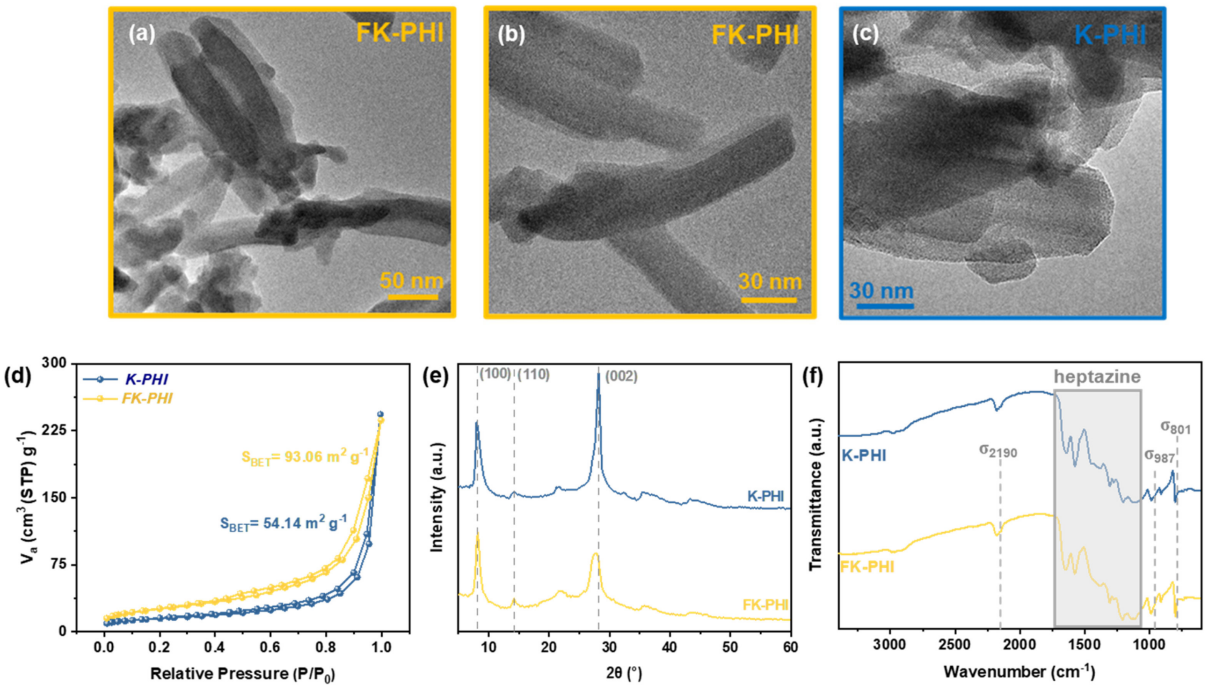

FIGURE 1 | HR-TEM micrographs recorded for (a,b) FK-PHI and (c) K-PHI; (d) N_2 adsorption–desorption isotherms of investigated samples, while the calculated BET specific surface area are displayed in the inset; (e) PXRD diffraction patterns recorded for carbon nitride analogs, with (100), (110), and (002) reflection modes of PHI appearing at 8.15°, 14°, and 28.2°(2θ), respectively; (f) FT-IR spectra recorded for investigated samples, with characteristic vibrational modes of PHI networks highlighted in the inset.

yellow-to-blue transition once the potential is swept beyond approximately −0.9 V versus Ag/Ag^+, as depicted in Figure 2a. This color change is accompanied by a pronounced cathodic current and is followed by an asymmetric anodic response upon reversal of the scan. It means that electrons introduced at negative bias remain temporarily stored in the film and are released only upon re-oxidation. The evolution of the CV thus directly links the electrochromic response to electrochemical charging of the PHI-based film. The onset potential (−0.9 V vs. Ag/Ag^+) overcomes the theoretical conduction band (CB) minimum of PHIs, i.e., the additional electrons are doped into the empty CB once the energy is sufficient [20]. Due to the increasing density of states in the CB, charges quickly accumulate into the film, accompanied by the development of characteristic blue color. To confirm the nature of this charged state, in-situ UV–vis spectroscopy was performed (Figure 2b). In the blue state, FK-PHI exhibits a broad absorption band centered around 600 nm, a spectral signature identical to that of the stable ionic species generated in carbon nitrides under illumination [25] without appropriate organic partners to reduce (photocharging).

These results establish that FK-PHI can be driven reproducibly into the characteristic blue reduced state by purely electrochemical means in organic media, without hole scavenger, providing the basis for quantitative analysis of its charge-stored response. The voltammetric response indicates a (pseudo)capacitive process: cathodic scanning generates negative currents that are partly recovered as anodic currents during the reverse sweep. The pronounced asymmetry further shows that charging and discharging proceed with different kinetics, while the amount of stored charge depends on the applied potential window. This is consistent with distinct charging regimes arising from a potential-dependent density of states that increases at more negative potentials.

2.3 | Charge Storage in FK-PHI

To quantify the charge-storage response of FK-PHI (electron accumulation capacity), the films were charged potentiostatically (chronoamperometry) for 30 s at progressively more negative potentials and then discharged galvanostatically at 100 mA g^{-1} (Figures S1 and 2c). Storage capacity has been quantified via integrating the discharge currents over time (see supplementary material and Equation S1). This protocol reveals a clear dependence of extracted charge on the charging bias. Above the onset potential for reduction, progressively more negative potentials lead to steadily increasing discharge capacity, as displayed in Figure 2d, reaching up to 82 C g^{-1} (853 µmol g^{-1}) after charging at −1.9 V versus Ag/Ag^+. In chemical terms, this corresponds to approximately one stored electron per 4.5 melem units, assuming an ideal poly(heptazine imide) structure, in which the molecular weight of a K-PHI monomer is 223 g mol^{-1} [8].

The shape of the discharge curves also evolves with charging potential. At lower charging bias, the discharge is dominated by a sloping profile reminiscent of (pseudo)capacitive storage, indicating toward a multi-factor mechanism governed by both charge

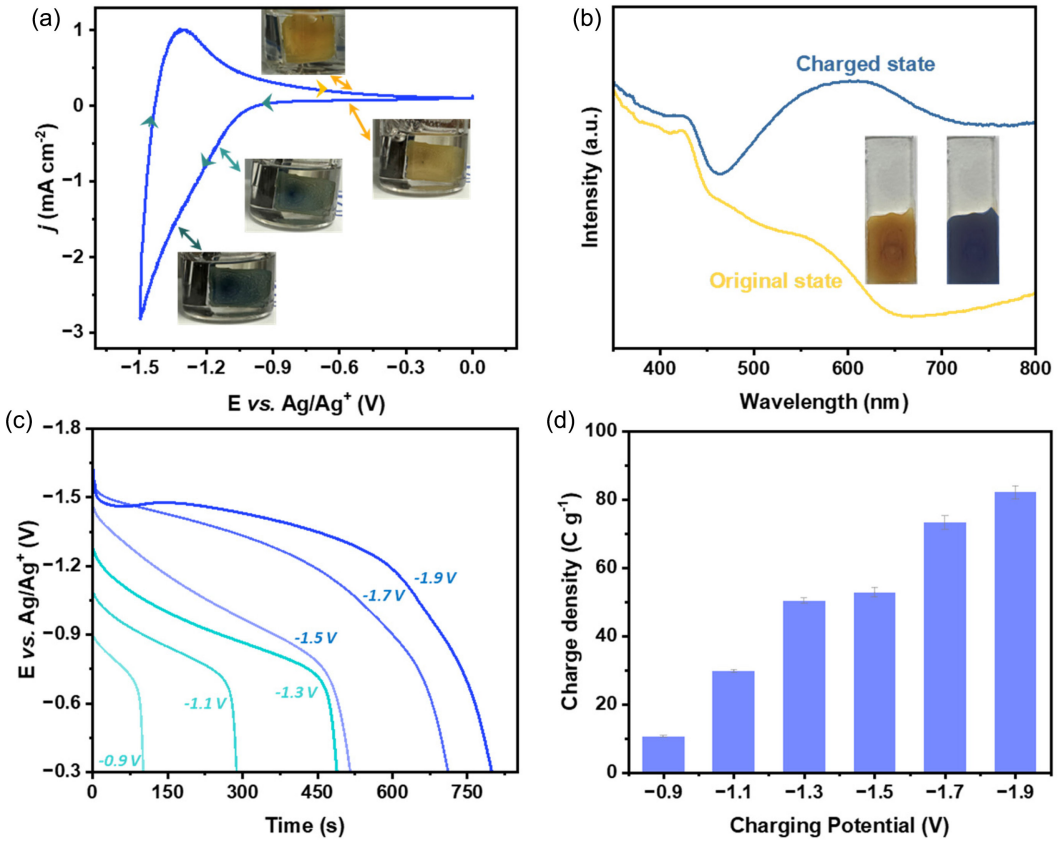

FIGURE 2 | (a) CV scan at 20 mV s^{-1} in 0.1 M $LiClO_4$ in acetonitrile under a potential window between 0 and −1.5 V versus Ag/Ag^+; (b) UV–vis spectra of FK-PHI under original state and charged state. (c) Discharge profiles at 100 mA g^{-1} showing increased charge storage after increasing charging potentials. (d) Extracted charge as a function of the corresponding electrode potential before the discharge and evaluation of the charge density resulting from the charge difference between the respectively attained voltage values.

insertion into the polymeric network, and ion diffusion/insertion for the electrostatic stabilization of said charges, whereas at more negative potentials a more pronounced plateau-like region emerges, which we propose as being an outcome of sluggish release of incorporated Li^+. This transition suggests that, at more negative charging potentials, charge release becomes increasingly dominated by states within a narrower potential range. At the same time, stable cycling is more readily maintained under milder charging conditions, whereas prolonged operation at strongly negative bias leads to partial film detachment from FTO, highlighting the difference between maximal apparent storage and the more robust operational window.

A peculiarity previously described for charge accumulation in PHI-networks is the long-lived nature of these e^-, thus enabling time-delayed redox processes. Thus, the herein described FK-PHI electrodes were charged for 30 s at −1.9V versus Ag/Ag^+, and further discharged after incremental delay times, ranging from 5 to 60 min (Figure S3a). Results indicate gradual charge losses, up to 83.5% after 1 h, potentially due to circuit losses, whereas 95% in the presence of O_2 after 5 min of exposure (Figure S3c). Therefore, compared to parallel photochemical approaches, where accommodated charges may persist for extended periods, up to days, electrochemical loading allows a narrower window for time-delayed processes.

To gain insights into the kinetic character of the discharging process, we analyzed the dependence of CV anodic peak current on scan rate using the power-law relationship between the anodic peak current (i_p) and the scan rate (v) (Figure S3a), according to Equation (1):

$$i_p = av^b \tag{1}$$

A linear fit of $\log(i_p)$ versus $\log(v)$ over a scan rate range of 10–100 $mV\,s^{-1}$ yielded a b-value of 0.61 (Figure S3 and Table S1), situated between the ideal limits of 0.5 (diffusion-controlled) and 1.0 (surface-controlled). This indicates that the electrochemical response contains both fast and slow contributions. We interpret this as a mixed charge-storage mechanism, where a fast surface-controlled process first introduces the electrons and counterions into the materials, followed by a significant diffusion-limited component toward the deeper layers of the materials, presumably by diffusion of the Li-ions through the structural micropores of PHI.

Additional support for this mixed kinetic behavior is provided by the pronounced hysteresis in the CV response and by impedance spectroscopy. The CV traces (Figure S4) show that electrons stored at negative potentials are not released immediately upon reversal of the scan, but require a broad return to more positive potentials before full deloading is achieved. Consistently, EIS measurements reveal a drastic reduction in charge–transfer resistance upon charging. Recorded Nyquist plots (Figure S5 and Table S2) reveal a reduction in the charge–transfer resistance from the MΩ range in the pristine state to a mere 91.2 Ω in the fully charged state. This provides evidence that electron injection improves the electronic conductivity of the FK-PHI film and lowers the barrier for interfacial charge transfer: the carbon nitride semiconductor is ionotronically doped. The kinetic bottleneck is the sluggish ion diffusion required for charge compensation, which is visually manifested as the discharge hysteresis in the CV scans.

A useful comparison can be drawn between photo- and electrochromic charging of PHI materials. Under photocatalytic conditions, K-PHI has previously been reported to store up to 92 $C\,g^{-1}$ after 24 h of irradiation in the presence of a hole scavenger, whereas in the present electrochemical approach, FK-PHI reaches comparable charge densities within seconds under applied bias. Although the two charging modes differ in operation, both are ultimately limited by the energetic accessibility of charge-storing states and by the onset of competing side reactions at more negative potentials. In our case, FK-PHI retained a stable discharge capacity of 29.7 $C\,g^{-1}$ when charged at −1.1 V, where decomposition processes are not yet activated, demonstrating good stability at moderate bias, while prolonged cycling at more negative potentials led to partial film detachment from the FTO support (Figure S2). It must be mentioned that related precedents of PHI-related electrochemical systems tackle electrode robustness through direct growth of carbon nitride films onto conductive substrates [26], strategy worth exploring for electrochemical loading of PHI, conditioned by controllable film thickness and crystalline consistency. Compared with earlier electrochemical charging of PHI in aqueous electrolyte, which reached about 45 $C\,g^{-1}$ at −0.75 V versus Ag/AgCl, the non-aqueous medium used here offers a wider cathodic window and thereby enables faster and more extensive charge accumulation.

Overall, the electrochemical behavior of FK-PHI in non-aqueous medium is consistent with a potential-dependent, ion-coupled electron-storage process in which charging enhances film conductivity but remains kinetically influenced by slower compensating-ion motion. In order to gain direct insight into the alterations of the band structure arising from electrochemical e^--Li^+ injection into the FK-PHI semiconductor, valence electron energy-loss spectroscopy (VEELS) surveys were acquired after deposition of the target specimen onto 4-finger gold electrodes designed for in-situ TEM investigation. Since the electron counts in EEL spectra are proportional to the local density of states of the probed volume, a semiconductor's electrical bandgap can be estimated by the onset of the valence-electron spectra in the low-loss (<50 eV) region. Additional experimental details are described in the supplementary material. It must be denoted that, due to operational conditions involving high vacuum of the analysis chamber, acetonitrile-based electrolytes could not be employed, and in turn $[EMIM^+][BF_4^-]$ was chosen as replacement due to its negligible volatility and relatively small ions. Thus, in order to check the feasibility of this chemical system in achieving PHI electrochromism, a 0.1M solution (in acetonitrile) containing the ionic liquid (IL) was charged for 30 s under diverse potentials, from −0.9 to −1.9V versus Ag/Ag^+ (Figure S6), yielding a maximum charge density of 19 $C\,g^{-1}$. Deposition of investigated K-PHI specimens onto the TEM chips, and further addition of IL into the system, is evidenced in Figure S7, while the intimate contact between solid specimen and IL is confirmed via EDX mapping of K (originating from K-PHI) and F (present via BF_4^- anions in the IL) species.

Probing the evolution of recorded bandgaps under different experimental conditions must consider potential physical and chemical interactions between specimen, IL, electrical bias, and electron beam. Therefore, FK-PHI was first investigated in absence of IL and bias, as shown in Figure S8. Fitting the linear region (2.7–3.2 eV) in the thinnest observed analysis region/cluster (Cluster 8),

resulted in an intercept with the baseline (i.e., highest point of the valence band) at 2.7 eV, value consistent with previously reported K-PHI related analogues. Thicker clusters show slightly lower values, with an average of 2.63 ± 0.1 eV. For FK-PHI in the presence of IL (Figure S9), in comparison with the isolated specimen, the bulk plasmons (10–35 eV) become predominant, and the features of the K-PHI surface plasmon (2–10 eV) are smeared out by the IL states and possibly by the long tail of the bulk excitations. According to previous reports [27] on experimental low-energy EELS, the valence spectrum of this IL exhibits a smooth start at around 4 eV, meaning that the bandgap determination by this technique should not be influenced. A fitting for Cluster 6 shows an intercept at 2.69 eV, while the average is 2.63 ± 0.1 eV. Both are consistent with the reference K-PHI. After applying −1.5V (1 V s^{-1} rate) to the in-situ chip containing both FK-PHI and IL, the spectra acquired show a shift of the onset potential, while new states are also evidenced (Figure S10). Comparison of the averaged EEL spectra for the described operational and acquisition conditions is illustrated in Figure 3a, while investigation over similar thickness of analyzed region is shown in Figure 3b. Though it would require a momentum-resolved EELS experiment to determine the band structure and possible transitions, this result is nevertheless consistent with a shift of the VB to 2.1 V, which is indicative of the presence of a larger population of electrons in the CB, which in turn also destabilizes to a minor extent the VB. The shift of the optical spectrum to a broader absorption contribution (Figure 2b) in the yellow–red region, observed ex-situ, is then in agreement with transitions of the new VB position to the CB. Cluster 7 gives an intercept of 2.16 eV, while the average is 2.03 ± 0.1 eV. Thus, a simplified band structure can be proposed for FK-PHI (Figure 3c), which explains the experimental observations. There are further changes in the VEELS spectra pointing to a separation into different smaller charged domains, as observed for the biased sample in Figure 2b, yet more definite analysis has to await detailed molecular modeling.

2.4 | The Charge-Storage Response is Governed by the Electrolyte Environment

A central objective of this work was to determine how the non-aqueous electrolyte environment regulates charge storage in FK-PHI. It is crucial to recognize that charge storage in the FK-PHI electrode occurs at a complex interface consisting of the conductive substrate, the semiconductor material, and the liquid electrolyte. Therefore, the charge transfer dynamics are governed not only by the electronic properties of the semiconductor, but are fundamentally coupled with the behavior of ions which need to migrate into the porous PHI, as well to the as-formed dynamic electrical double layer at the solid–liquid interface. Electron injection and ion compensation are synergistic and inseparable processes. The properties of the cation and its surrounding solvent shell act as a powerful external lever to regulate the overall storage kinetics and capacity.

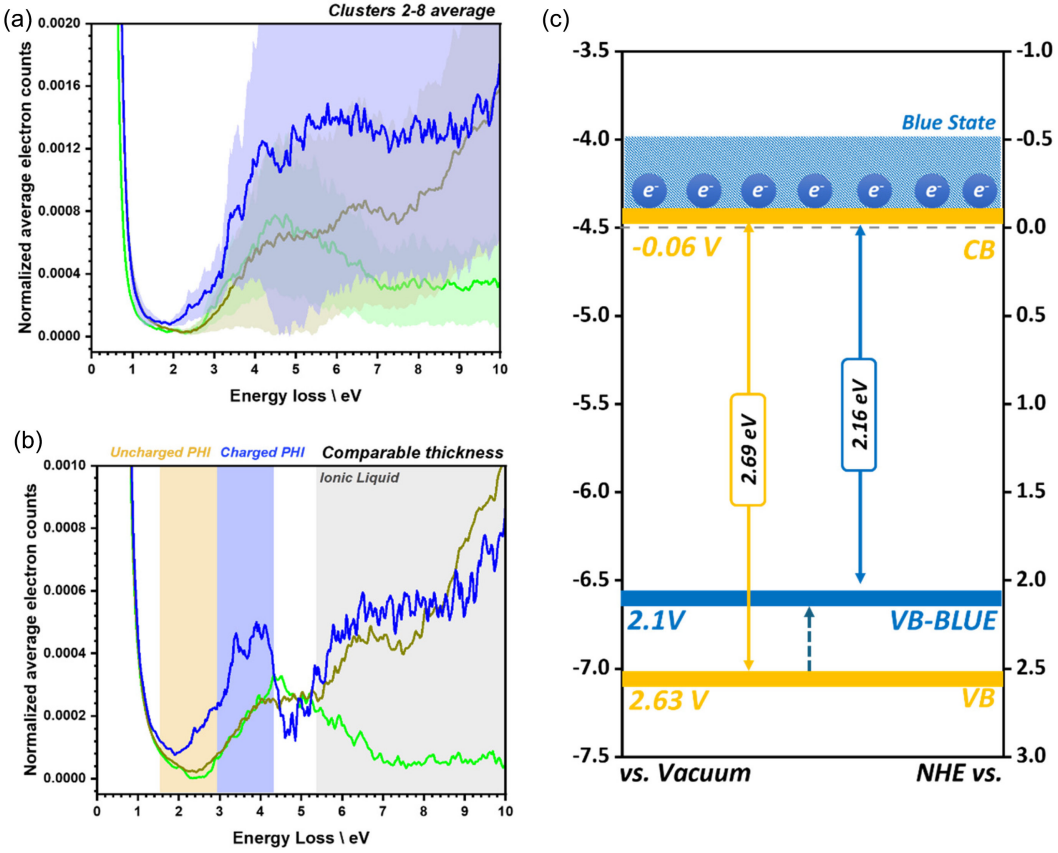

FIGURE 3 | (a) Average of acquired EEL spectra for K-PHI (green), K-PHI in IL (brown), and biased K-PHI in IL (blue) over different scanning regions from inner to outer parts of selected analysis regions; (b) comparison between K-PHI (green), K-PHI in IL (brown), and biased K-PHI in IL (blue) over comparable thicknesses of analyzed regions; (c) proposed band structure for FK-PHI and the induced VB energy level shift as a consequence of charging, the VB maxima value being adopted from related literature precedents [28, 29].

Comparative electrochemical studies were performed in electrolytes containing Li^+, Na^+, and TBA^+ cations with the same ClO_4^- anion. As shown in Figure 4a, smaller cations such as Li^+ and Na^+ promote more efficient diffusion into the structural cavities of K-PHI, thereby enhancing charge storage and lead to a more pronounced color change (grades of blue). In contrast, the bulky TBA^+ primarily contributes to double-layer capacitance rather than intercalation. This trend was observed across all potentials in the range tested (Figure 4b), as charge densities of 54, 42, and 12 C g^{-1} were obtained for Li^+, Na^+, and TBA^+, respectively, after charging at −1.5 V (vs. Ag/Ag+) for 30 s and discharging at a rate of 100 mA g^{-1}. Notably, considering the solvated forms of investigated cations, FK-PHI charge stabilization shows a clearly distinguishable preference for Li^+ moieties, despite having a comparable or slightly larger size than that of Na^+ (solvated radius of ~4.8 and ~4.6 Å, respectively), while the size TBA^+ (solvated radius of ~5.3 Å) is beyond the range of incorporation and is expected to inhibit the process [30–32]. This strong cation dependence indicates that the compensating ion is not a passive spectator but an integral part of the charging process. Smaller inorganic cations support substantially more efficient charge stabilization than the bulky TBA^+ species, which appears to contribute mainly to interfacial charging without enabling efficient storage in the PHI film. In order to probe whether K^+ ions present in the K-PHI ionic structure are unaffected by these charge/discharge cycles, post-process ICP analysis was carried out. As-synthesized FK-PHI incorporates K^+ ions up to 9.91 wt.%, while trace amounts of Li^+ are also present (0.2 wt%), due to the salt flux synthetic process. After electrochemical processing, K^+ content decreased to 3.11 wt%, while a notable Li^+ content of 2.64 wt% was detected. Thus, these results indicate a dynamic exchange between K^+ and Li^+ during electrochemical loading, further evidencing that charge uptake is directly dependent on ion diffusibility through the structural channels of PHI.

To understand whether observed organic cation effects were influenced by solvent identity, parallel studies to those performed in acetonitrile were done in dimethyl sulfoxide and propylene carbonate, as shown in Figure S11. When the same salts were examined in different solvents, the charging response decreased

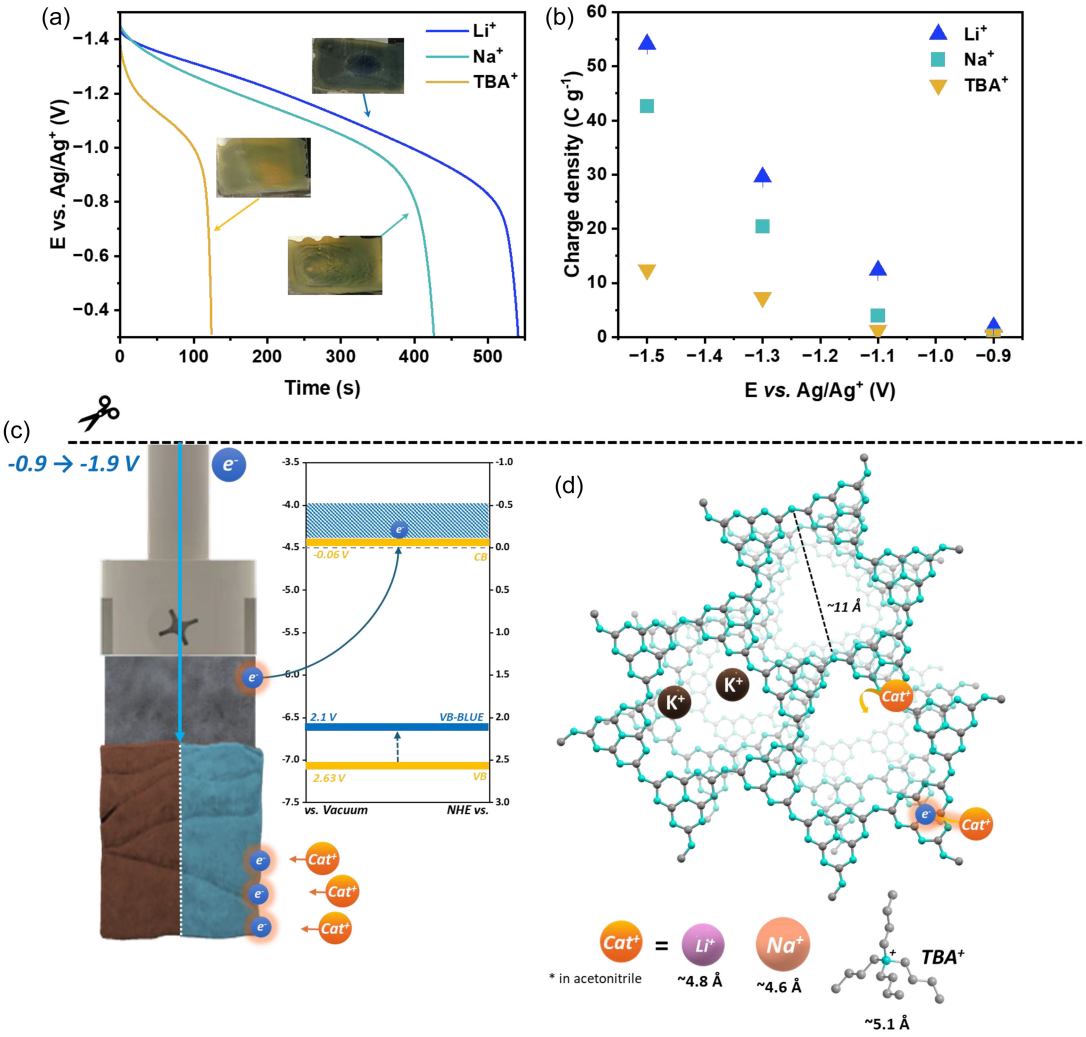

FIGURE 4 | (a) Discharge curves of FK-PHI in 0.1 M $LiClO_4$, $NaClO_4$, and $TBAClO_4$ in acetonitrile at 100 mA g^{-1}; (b) charge extraction of FK-PHI from −0.9 to −1.5 V versus Ag/Ag^+ in 0.1 M $LiClO_4$, $NaClO_4$, and $TBAClO_4$ in acetonitrile; (c) Tafel plots of in 0.1 M $LiClO_4$, $NaClO_4$, and $TBAClO_4$ in acetonitrile calculated from the LSV curves in Rotating Disk Electrode Measurement at 900 rpm; (d) schematic illustration of our proposed mechanism for FK-PHI electrochromism, and different factors influencing the process. The K-PHI structural model displays C atoms in gray and N atoms in cyan, while H atoms are excluded for the sake of visual clarity. Solvated cationic radii are adopted from literature [30–32].

with increasing dielectric strength of the medium, effect which we attribute to enlarged solvation shells and detrimental charge shielding, thus limiting both diffusion of cations into the PHI matrix, as well as effective Coulombic stabilization of injected charges [33, 34]. Likewise, increasing the electrolyte concentration from 0.1 to 1 M did not improve storage but instead reduced charging efficiency, particularly for larger cations (Figure S12). Together, these observations point to an important role of ion pairing, solvation, and desolvation at the interface [35, 36]. In other words, charge storage in FK-PHI is controlled not only by the redox energetics of the solid, but also by how readily the surrounding electrolyte can supply effective compensating cations under bias.

On the basis of these observations, a working picture for charging in FK-PHI can be proposed. Cathodic bias injects electrons into the PHI framework, populating electronic levels in the conduction band of KF-PHI, as described through recorded EEL, leading to the formation of the characteristic blue reduced state. We propose that charging occurs via direct electron injection into the semiconductor, this behavior being directed by the magnitude of applied bias potential. Charge accumulation is then stabilized by compensating cations supplied from the electrolyte, and the efficiency of this coupled ion-electron process depends strongly on cation size, solvation, and electrolyte composition. The discharge behavior and attainable stored charge therefore emerge from an interplay between the electronic structure of FK-PHI and the physicochemical properties of the surrounding non-aqueous medium.

These results identify the electrolyte as an active design parameter for electrochemical PHI charging. Rather than merely extending the cathodic window relative to water, the non-aqueous medium directly controls how efficiently the reduced blue state can be generated, stabilized, and accessed electrochemically.

3 | Conclusion

In summary, we have established a purely electrochemical method to control and quantify the intrinsic charge storage in an FK-PHI electrode, achieving a high capacity of 82 $C\,g^{-1}$ at a rate that is orders of magnitude faster than conventional photocharging. Our comprehensive analysis reveals that this process is governed by an ion-electron pair integration mechanism. In-situ EELS experiments bring clarity into the electronic alternations of the PHI semiconductor and the energy levels at which additional charges are accommodated. Crucially, this work demonstrates that the entire energy storage process is exquisitely regulated by the external electrochemical environment, where cation size and solvent polarity dictate the interfacial and intercalation kinetics. Besides charge storage, several beneficial properties may accompany this blue-state of carbon nitride, with important implications in transition states and catalytic turnovers, not to mention about improved spectral coverage of solar contributions, which in turn might facilitate chemical reactions.

Acknowledgments

The authors gratefully acknowledge the Max Planck Society for financial support. Moreover, authors sincerely thank Katharina ten Brummelhuis, Ursula Lubahn, Jessica Brandt, and Bolortuya Badamdorj from Max Planck Institute of Colloids and Interfaces for technical support. A.K. acknowledges funds from the Fonds voor Wetenschappelijk Onderzoek – Vlaanderen (FWO) for the travel grant for long stay abroad (No. V430226N).

Open Access funding enabled and organized by Projekt DEAL.

Funding

This study was supported by Max-Planck-Gesellschaft.

Conflicts of Interest

The authors declare no conflicts of interest.

Data Availability Statement

Data associated with the in-situ EELS investigation and methodology is available free of charge on Edmond – the Open Research Data Repository of the Max Planck Society (https://doi.org/10.17617/3.ASOTQR). Other datasets associated with this study are available upon request from authors.

References

1. X. Wang, K. Maeda, A. Thomas, et al., "A Metal-Free Polymeric Photocatalyst for Hydrogen Production from Water under Visible Light," *Nature Materials* 8, no. 1 (2009): 76–80, https://doi.org/10.1038/nmat2317.

2. X. Luo, Y. Zhai, P. Wang, et al., "Light-Mediated Polymerization Catalyzed by Carbon Nanomaterials," *Angewandte Chemie International Edition* 63, no. 18 (2024): e202316431, https://doi.org/10.1002/anie.202316431.

3. C. Wang, J. Zhuang, and O. Savateev, "Organic Synthesis Mediated by Carbon Nitride Photocatalysis and Photocharged Carbon Nitrides," *Accounts of Chemical Research* 59, no. 2 (2026): 246–257, https://doi.org/10.1021/acs.accounts.5c00687.

4. G. A. A. Diab, I. F. Reis, C. Wang, et al., "Ionic Metal Poly(Heptazine Imides) and Single-Atoms Interplay: Engineered Stability and Performance for Photocatalysis, Photoelectrocatalysis and Organic Synthesis," *Advanced Functional Materials* 35, no. 44 (2025): 2501393, https://doi.org/10.1002/adfm.202501393.

5. Y. Zheng, Z. Hang, J. Ouyang, and Z. Chen, "Hierarchical Design of 2D Carbon Nitride and Derivatives for Next-Generation Energy Conversion and Storage Technologies," *Small* 21, no. 37 (2025): e05924, https://doi.org/10.1002/smll.202505924.

6. G. Chan, D. Corsi, O. Savateev, P. Giusto, and J. P. Barham, "Interfacial Photoelectrochemistry in Organic Synthesis," *Angewandte Chemie International Edition* 64, no. 42 (2025): e202424300, https://doi.org/10.1002/anie.202424300.

7. A. Actis, M. Melchionna, G. Filippini, et al., "Singlet-Triplet Energy Inversion in Carbon Nitride Photocatalysts," *Angewandte Chemie International Edition* 62, no. 48 (2023): e202313540, https://doi.org/10.1002/anie.202313540.

8. Y. Markushyna, P. Lamagni, C. Teutloff, et al., "Green Radicals of Potassium Poly(Heptazine Imide) Using Light and Benzylamine," *Journal of Materials Chemistry A* 7, no. 43 (2019): 24771–24775, https://doi.org/10.1039/C9TA09500D.

9. A. Rogolino and O. Savateev, "Photochargeable Semiconductors: In 'Dark Photocatalysis' and Beyond," *Advanced Functional Materials* 33, no. 45 (2023): 2305028, https://doi.org/10.1002/adfm.202305028.

10. H. Schlomberg, J. Kröger, G. Savasci, et al., "Structural Insights into Poly(Heptazine Imides): A Light-Storing Carbon Nitride Material for Dark Photocatalysis," *Chemistry of Materials* 31, no. 18 (2019): 7478–7486, https://doi.org/10.1021/acs.chemmater.9b02199.

11. V. W. Lau, D. Klose, H. Kasap, et al., "Dark Photocatalysis: Storage of Solar Energy in Carbon Nitride for Time-Delayed Hydrogen Generation," *Angewandte Chemie* 129, no. 2 (2017): 525–529, https://doi.org/10.1002/ange.201608553.

12. C. Wang, J. Zhuang, Z. Xie, et al., "Decoupled Solar Energy Conversion and Charge Storage in a Carbon-Doped Sodium Poly(Heptazine Imine) for Dark Photocatalysis," *Small Structures* 7, no. 1 (2026): e202500706, https://doi.org/10.1002/sstr.202500706.

13. H. Szalad, A. Galushchinskiy, T. Jianu, et al., "Polymeric Triazine/Heptazine Imide Heterostructures Enable Photocatalytic O_2 Reduction to H_2O_2," *Applied Catalysis B: Environment and Energy* 357 (2024): 124323, https://doi.org/10.1016/j.apcatb.2024.124323.

14. Y. Wang, M. Yang, Y. Wang, and J. Cheng, "Cyanamide-Functionalized Carbon Nitride with Ion Modification for Enhanced 'Dark' Photocatalysis," *Advanced Functional Materials* 35, no. 31 (2025): 2503353, https://doi.org/10.1002/adfm.202503353.

15. S. Mazzanti, C. Schritt, K. ten Brummelhuis, M. Antonietti, and A. Savateev, "Multisite PCET with Photocharged Carbon Nitride in Dark," *Exploration* 1, no. 3 (2021): 20210063, https://doi.org/10.1002/EXP.20210063.

16. F. Podjaski, J. Kröger, and B. V. Lotsch, "Toward an Aqueous Solar Battery: Direct Electrochemical Storage of Solar Energy in Carbon Nitrides," *Advanced Materials* 30, no. 9 (2018): 1705477, https://doi.org/10.1002/adma.201705477.

17. L. O. S. Colbin, Y. Shao, and R. Younesi, "Ion-Pairing: A Bygone Treatment of Electrolyte Solutions?," *Batteries \& Supercaps* 8, no. 1 (2025): e202400160, https://doi.org/10.1002/batt.202400160.

18. C. G. Swain, M. S. Swain, A. L. Powell, and S. Alunni, "Solvent Effects on Chemical Reactivity. Evaluation of Anion- and Cation-Solvation Components," *Journal of the American Chemical Society* 105, no. 3 (1983): 502–513, https://doi.org/10.1021/ja00341a033.

19. M. Wang and Z. Feng, "Interfacial Processes in Electrochemical Energy Systems," *Chemical Communications* 57, no. 81 (2021): 10453–10468, https://doi.org/10.1039/D1CC01703A.

20. A. Savateev, N. V. Tarakina, V. Strauss, et al., "Potassium Poly(Heptazine Imide): Transition Metal-Free Solid-State Triplet Sensitizer in Cascade Energy Transfer and [3+2]-Cycloadditions," *Angewandte Chemie International Edition* 59, no. 35 (2020): 15061–15068, https://doi.org/10.1002/anie.202004747.

21. Z. Chen, A. Savateev, S. Pronkin, et al., "The Easier the Better' Preparation of Efficient Photocatalysts—Metastable Poly(Heptazine Imide) Salts," *Advanced Materials* 29, no. 32 (2017): 1700555, https://doi.org/10.1002/adma.201700555.

22. T. S. Miller, A. B. Jorge, T. M. Suter, A. Sella, F. Corà, and P. F. McMillan, "Carbon Nitrides: Synthesis and Characterization of a New Class of Functional Materials," *Physical Chemistry Chemical Physics* 19, no. 24 (2017): 15613–15638, https://doi.org/10.1039/C7CP02711G.

23. V. Shvalagin, N. Tarakina, B. Badamdorj, et al., "Simultaneous Photocatalytic Production of H2 and Acetal from Ethanol with Quantum Efficiency over 73% by Protonated Poly(Heptazine Imide) under Visible Light," *ACS Catalysis* 14, no. 19 (2024): 14836–14854, https://doi.org/10.1021/acscatal.4c04180.

24. A. Galushchinskiy, C. Pulignani, H. Szalad, et al., "Heterostructured PHI-PTI/Li^+Cl^- Carbon Nitrides for Multiple Photocatalytic Applications," *Solar RRL* 7, no. 14 (2023): 2300077, https://doi.org/10.1002/solr.202300077.

25. G. Zhang, G. Li, Z.-A. Lan, et al., "Optimizing Optical Absorption, Exciton Dissociation, and Charge Transfer of a Polymeric Carbon Nitride with Ultrahigh Solar Hydrogen Production Activity," *Angewandte Chemie International Edition* 56, no. 43 (2017): 13445–13449, https://doi.org/10.1002/anie.201706870.

26. J. Su, J. Zhang, S. Chai, Y. Wang, S. Wang, and Y. Fang, "Optimizing Poly(Heptazine Imide) Photoanodes Using Binary Molten Salt Synthesis for Water Oxidation Reaction," *Acta Physico-Chimica Sinica* 40, no. 12 (2024): 2408012, https://doi.org/10.3866/PKU.WHXB202408012.

27. K. Regeta, C. Bannwarth, S. Grimme, and M. Allan, "Free Electrons and Ionic Liquids: Study of Excited States by Means of Electron-Energy Loss Spectroscopy and the Density Functional Theory Multireference Configuration Interaction Method," *Physical Chemistry Chemical Physics* 17, no. 24 (2015): 15771–15780, https://doi.org/10.1039/C5CP01417D.

28. H. Tong, J. Odutola, J. Song, et al., "Boosting the Quantum Efficiency of Ionic Carbon Nitrides in Photocatalytic H_2O_2 Evolution via Controllable $n \rightarrow \Pi^*$ Electronic Transition Activation," *Advanced Materials* 36, no. 49 (2024): 2412753, https://doi.org/10.1002/adma.202412753.

29. C. M. Pelicano, J. Li, M. Cabrero-Antonino, et al., "Rational Design of a Carbon/Potassium Poly(Heptazine Imide) Heterojunction for Enhanced Photocatalytic H_2 and H_2O_2 Evolution," *Journal of Materials Chemistry A* 12, no. 1 (2024): 475–482, https://doi.org/10.1039/D3TA05701A.

30. D. M. Seo, P. D. Boyle, O. Borodin, and W. A. Henderson, "Li^+ Cation Coordination by Acetonitrile—*2*014; Insights from Crystallography," *RSC Advances* 2, no. 21 (2012): 8014–8019, https://doi.org/10.1039/C2RA21290K.

31. D. Spångberg and K. Hermansson, "The Solvation of Li^+ and Na^+ in Acetonitrile from Ab Initio-Derived Many-Body Ion–Solvent Potentials," *Chemical Physics* 300, no. 1 (2004): 165–176, https://doi.org/10.1016/j.chemphys.2004.01.011.

32. N. G. Tsierkezos and A. I. Philippopoulos, "Studies of Ion Solvation and Ion Association of N-Tetrabutylammonium Hexafluorophosphate and n-Tetrabutylammonium Tetraphenylborate in Various Solvents," *Fluid Phase Equilibria* 277, no. 1 (2009): 20–28, https://doi.org/10.1016/j.fluid.2008.11.004.

33. X. Hu, Q. Lin, J. Gao, Y. Wu, and Z. Zhang, "Anion–Cation and Ion–Solvent Interaction of Some Typical Ionic Liquids in Solvents with Different Dielectric Constant," *Chemical Physics Letters* 516, no. 1 (2011): 35–39, https://doi.org/10.1016/j.cplett.2011.09.051.

34. P. C. do Couto and D. M. Chipman, "How Does Dielectric Solvation Affect the Size of an Ion?," *The Journal of Physical Chemistry A* 114, no. 48 (2010): 12788–12793, https://doi.org/10.1021/jp108873z.

35. X. Yu, M. Chen, J. Wang, et al., "Deciphering Multi-Dimensional Interfacial Mechanisms via Organic Cosolvent Engineering for Sustainable Zinc Metal Batteries," *Nature Communications* 16, no. 1 (2025): 3820, https://doi.org/10.1038/s41467-025-59069-7.

36. S. Sawayama, M. Matsugami, and K. Fujii, "Direct Molecular Evidence for Desolvation-Controlled Lithium-Ion Insertion at Graphite Electrodes in Highly Concentrated Electrolytes," *The Journal of Physical Chemistry Letters* 16, no. 36 (2025): 9334–9338, https://doi.org/10.1021/acs.jpclett.5c02274.

Supporting Information

Additional supporting information can be found online in the Supporting Information section.